agriculture

MDPI

Article

Optimizing the Strategies of *Ziziphus jujuba* 'Dongzao' Irrigation with Long-Term Saline Water in Yellow River Delta, China, Using MODFLOW and HYDRUS-2D

Xin Cong [1], Yucai Xie [1], Rongzhen Wang [2], Zhenghe Xu [1,3,*] and Guibin Pang [1]

[1] School of Water Conservancy and Environment, University of Jinan, Jinan 250022, China; stu_congx@ujn.edu.cn (X.C.)
[2] Rural Vitalization Research Institute, Shandong Agriculture and Engineering University, Jinan 250100, China
[3] Shandong Key Laboratory of Eco-Environmental Science for the Yellow River Delta, Shandong University of Aeronautics, Binzhou 256600, China
* Correspondence: stu_xuzh@ujn.edu.cn

Abstract

Optimizing saline drip irrigation to protect soil conditions and maintain *Ziziphus jujuba* 'Dongzao' yield is critical for freshwater-scarce regions with shallow saline groundwater. This study incorporated groundwater table variations and their long-term effects into the irrigation scheduling optimization framework to develop a saline drip irrigation regulation pattern suitable for jujube under shallow groundwater conditions. To this end, simulated hydraulic heads from MODFLOW were used to update the bottom boundary condition of HYDRUS-2D, to quantify soil water–salt transport and optimize irrigation management. A three-year field experiment was conducted in the Yellow River Delta. Five saline drip irrigation treatments (1 (control), 2, 3, 4, and 5 g·L^{-1}) were established to investigate their influences on soil water content, soil salinity, jujube yield and fruit quality. Based on the experimental data, the MODFLOW and HYDRUS models were then calibrated and validated to simulate different saline water irrigation scenarios over a 10-year period, and the effects on the spatiotemporal variations in water and salt transport processes were analyzed. The main results were as follows: (1) The yield exhibited an inverse relationship with irrigation water salinity, with significant yield reductions ($p < 0.05$) observed only at the 4 and 5 g·L^{-1} treatments compared to the control. (2) The relative yield declined to 50% and 85% when the average saturated paste extract electrical conductivity (EC_e) of soil reached 12.64 dS·m^{-1} (0.27%) and 8.85 dS·m^{-1} (0.19%), respectively. Moderate saline irrigation improved fruit quality, and the treatment of 4 g·L^{-1} achieved the best performance. (3) For consecutive dry years, the seasonal total irrigation quota is 216–240 mm, with 3 g·L^{-1} as the baseline irrigation salinity and selected irrigation events adjustable down to 2 g·L^{-1}; for normal water years, the seasonal total irrigation quota is 168–192 mm with a constant irrigation salinity of 3 g·L^{-1} across the whole growing season; and, for consecutive wet years, the seasonal total irrigation quota is 72–96 mm, with 3 g·L^{-1} as the baseline irrigation salinity and selected irrigation events adjustable up to 4 g·L^{-1}. The research provides decision support for utilizing shallow saline groundwater to sustain 'Dongzao' jujube production.

Keywords: saline water drip irrigation; soil water and salt movement; yield and quality; model simulation; optimize irrigation scheme

Check for updates

Academic Editor: Margarita García-Vila

Received: 10 October 2026
Revised: 8 November 2026
Accepted: 12 November 2026
Published: 18 November 2026

Copyright: © 2026 by the authors. Licensee MDPI, Basel, Switzerland. This article is an open access article distributed under the terms and conditions of the Creative Commons Attribution (CC BY) license.

1. Introduction

In China, the improvement and sustainable utilization of saline–alkali land, together with agricultural water conservation, have become important priorities for ensuring food security and promoting sustainable agricultural development [1]. The Yellow River Delta (YRD), a critical ecological zone and major agricultural production base in China, faces significant constraints on high-quality agricultural development due to the severe freshwater scarcity and widespread soil salinization [2]. Studies demonstrate that shallow groundwater in most parts of the YRD is predominantly brackish or saline, except in certain areas of the southern interior [3]. The rational utilization of brackish groundwater for agricultural irrigation provides a potential approach to alleviating freshwater shortages in saline–alkali regions [4]. In this context, the use of brackish water for irrigation has become an important strategy to alleviate agricultural water shortages in the region. *Ziziphus jujuba* 'Dongzao' is an essential crop with high nutritional value and unique taste; its primary cultivation is concentrated in the Yellow River Delta [5]. Achieving the dual objectives of sustainable yield and high fruit quality in *Ziziphus jujuba* 'Dongzao' production under water-limited conditions remains a significant agronomic challenge. Research has shown that, under scientific irrigation management, brackish and saline water irrigation of appropriate mineralization can effectively substitute for freshwater in agriculture without significantly harming the soil and crop yield and enhancing crop quality [6,7]. A meta-analysis of 1108 comparisons from 39 studies on deficit irrigation in saline–alkali regions of China indicates that using slightly brackish water (0.7–2.0 $dS \cdot m^{-1}$) with an irrigation proportion of 0.85–0.9 crop evapotranspiration is more likely to achieve a trade-off among soil salinity content, crop yield, and IWP [8]. Zhao et al. [9] investigated the use of saline water (1–10 $g \cdot L^{-1}$) for irrigating gray jujube in Xinjiang and reported that short-term irrigation with low-salinity water ($\leq$3 $g \cdot L^{-1}$) enhanced growth and increased the yield, whereas long-term irrigation with highly saline water reduced both yield and water productivity. These studies consistently indicate that short-term irrigation with slightly saline water can alleviate the adverse effects of water stress on crops. However, if improper saline water irrigation strategies are used for a long time, it can easily lead to soil salt accumulation, resulting in a decrease in crop yield [10]. Currently, mature saline water irrigation strategies have been mainly applied to crops such as cotton [11], maize, and wheat [12], while their application to *Ziziphus jujuba* 'Dongzao' still requires further investigation. Furthermore, owing to the shallow groundwater table in the region, the accumulation of soluble salts in the soil is directly related to groundwater salinity and depth [13]. The interactive effects of groundwater depth and irrigation water salinity on soil salt accumulation during long-term slightly saline water irrigation remain poorly understood.

In addition to irrigation water salinity, irrigation scheduling, including irrigation timing, frequency, and quota, exerts a critical control over soil water–salt dynamics [14]. The performance of brackish water irrigation is further modulated by precipitation, groundwater conditions, and crop water requirements, which underscores the necessity of developing site-specific irrigation strategies adapted to variable hydrological conditions [15]. Although field experiments are commonly adopted to investigate irrigation impacts on groundwater head, soil water content, soil salinity, and crop growth, such experiments are generally labor-intensive, expensive, and limited in spatial and temporal applicability. Numerical models offer a powerful alternative to overcome these limitations, enabling predictions of long-term soil water and salinity dynamics at the regional scale [16]. For this reason, many researchers combine field observations with numerical simulations to derive optimal irrigation regimes that match local hydrogeological settings. The HYDRUS model simulates water, heat and solute transport processes in variably saturated porous media in two and three dimensions [17]. Additionally, it incorporates root water uptake, evapotranspiration

and transpiration processes [18]. For example, Zhang et al. [19] used HYDRUS (2D/3D) to optimize irrigation strategies with the alternate use of fresh and brackish waters in Hetao Irrigation District, China. Guo [7] used HYDRUS-3D to simulate three-dimensional soil water and salinity movement under brackish drip irrigation and optimized a strategy for overlaying brackish drip irrigation in Xinjiang, China. However, these optimizations are based on simulation results spanning 2–3 years and do not account for the cumulative effects of salt accumulation under long-term saline irrigation. Furthermore, research indicates that, in shallow groundwater zones, the groundwater level is the primary factor influencing soil water–salt dynamics [20]. Visual MODFLOW is one of the most powerful numerical simulation tools widely used to predicted groundwater flow movements. For example, Varouchakis et al. [21] applied Visual MODFLOW to assess the irrigation scenario and precipitation impacts on the groundwater resources of Viannos Basin at the island of Crete, Greece. Liu et al. [22] used Visual MODFLOW to assess the effects of different drainage channel designs on the groundwater head in the Yellow River Delta region. Luo et al. [23] applied Visual MODFLOW to investigate groundwater level responses and recovery processes following extreme precipitation events in the Yellow River Delta, highlighting the influence of precipitation on groundwater dynamics.

Hence, this study integrates field observations with numerical simulations. MODFLOW 2011 v4.6 is employed to simulate groundwater head dynamics, whose outputs are then imported into HYDRUS (2D/3D) v2.05 to drive simulations of soil water content (SWC) and soil salt concentration (SSC) under different irrigation water salinity regimes. The overall aim is to develop long-term brackish water irrigation strategies for *Ziziphus jujuba* 'Dongzao' adapted to the Yellow River Delta (YRD). The three objectives of this study are as follows: (1) to evaluate the soil water–salt transport dynamics, yield and fruit quality of jujube under varying irrigation water salinities; (2) to calibrate and validate the model using multiple types of data, including soil water, salts, and groundwater heads; and (3) to assess the long-term soil environmental impacts of alternative irrigation schemes, incorporating soil water and salinity stress thresholds of jujube. This study contributes to optimizing strategies of *Ziziphus jujuba* 'Dongzao' in the YRD regions, which are much needed for regional sustainability.

2. Materials and Methods

2.1. Field Experiments

The experiment was conducted from 2020 to 2022 during jujube growth period. The experimental site is located at the plot (37°42′36″ N–37°43′12″ N, 117°53′24″ E–117°54′36″ E), Zhanhua City, Shandong, with elevation of 3.0–8.0 m above the sea level and groundwater depth of 1.2–3 m. The area has a typical temperate monsoon climate with an annual precipitation of approximately 554 mm. The meteorological data for the experimental area during the jujube growth periods was presented in Figure 1. The long-term average groundwater level in this area is 3.9 m, with groundwater salinity of 3–5 $g \cdot L^{-1}$. According to the World Reference Base for Soil Resources (WRB), the soil at this site is classified as Gleyic Solonchaks [24]. Prior to the experiment, we randomly selected 15 points within the experimental plot and measured soil bulk density at various depths, along with the content of soil salinity and organic matter (Table 1). The soil of the study area is classified as Gleyic Solonchaks according to the WRB classification system.

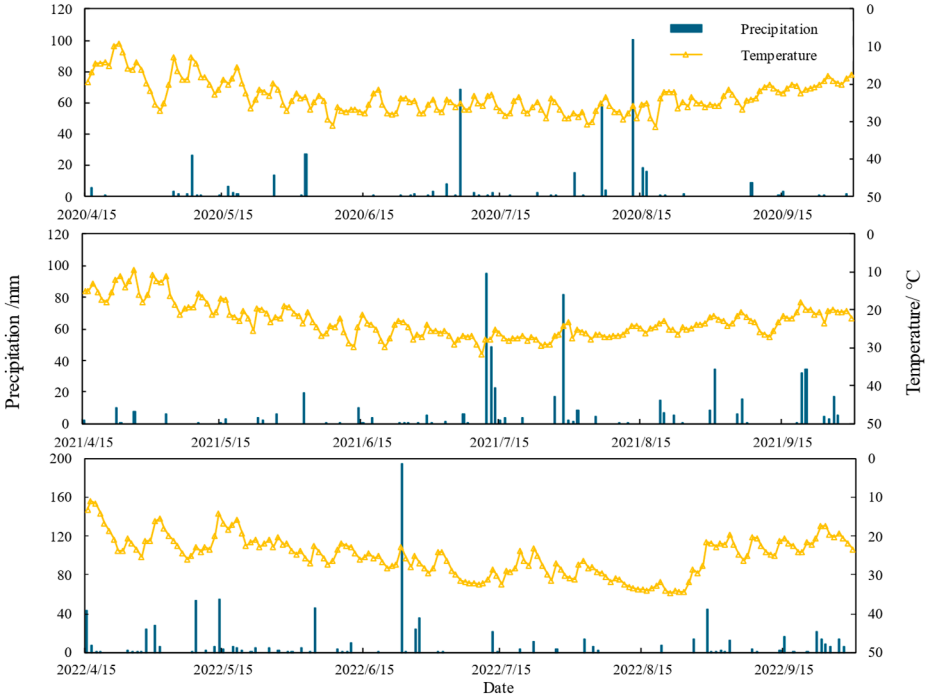


Figure 1. Meteorological data during the test period.

Table 1. Physical and chemical properties of the initial soils at the experimental sites.

Soil Layer (cm)	Soil Texture	Bulk Density ($g \cdot cm^{-3}$)	Field Capacity (%)	Soil Salinity ($g \cdot kg^{-1}$)	pH (1:5)	Soil Organic Matter ($g \cdot cm^{-3}$)
0–20	Loam	1.39	26.10	1.32	8.07	12.88
20–40	Sandy loam	1.56	27.50	2.45	8.39	12.65
40–60	Sandy loam	1.52	29.40	1.63	8.53	12.01
60–80	Loamy sandy	1.60	29.10	1.06	8.59	11.81
80–100	Loam	1.43	28.70	1.08	8.60	11.84

The experiment was set up with five treatments of irrigation water mineralization of 1, 2, 3, 4 and 5 $g \cdot L^{-1}$. The drip irrigation system employed a planting pattern consisting of one drip irrigation line per row of jujube trees, and the drip irrigation lines utilized were pressure-compensating drip tapes. Each treatment had three jujube rows as replicates. The in-row spacing of jujube trees was 2 m, and the row spacing was 3 m. Each experimental plot covered an area of 22 m × 9 m (Figure 2). Saline water was prepared by blending local shallow groundwater with freshwater (tap water). The salinity of the mixed irrigation water was measured using a multi-parameter water quality instrument (HQ30d, Hach Water Quality Analyzer Shanghai Co., Ltd., Shanghai, China). The volume of irrigation water was measured using a water meter. All treatments received uniform irrigation and fertilization, with fertilizer application rates of 750 $kg \cdot hm^{-2}$ nitrogen (N), 330 $kg \cdot hm^{-2}$ phosphorus pentoxide (P_2O_5), and 980 $kg \cdot hm^{-2}$ potassium oxide (K_2O). Following previous research by the team [25], the irrigation quota has been reduced by 10% and set to 24 mm. The specific irrigation schedule can be found in Table 2. Other field management practices, including weeding, and insect control, adhered to local farming traditions. Eleven pumping wells in the area monitored groundwater parameters (Figure 2).

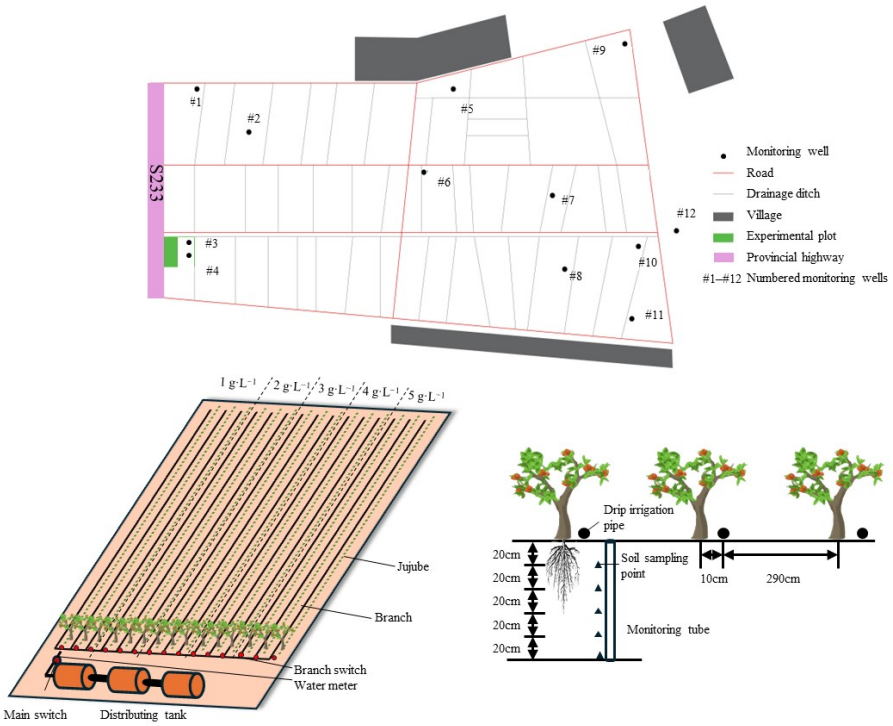


Figure 2. Distribution of monitoring sites and test plots in the study area.

Table 2. Irrigation regime and precipitation for each growth stage from 2020 to 2022.

Year	Item	Leaf Expansion Stage	Flowering and Fruiting Stage	Fruit Swelling Stage	Maturity Stage	Entire Growth Season
2020	Irrigation times	2	2	2	1	7
	Irrigation amount (mm)	48	48	48	24	168
	Precipitation (mm)	70.5	57.6	244.9	55.3	428.3
2021	Irrigation times	2	1	1	0	4
	Irrigation amount (mm)	48	24	24	0	96
	Precipitation (mm)	60.3	124.8	268.4	120.1	573.6
2022	Irrigation times	1	2	1	1	5
	Irrigation amount (mm)	24	48	24	24	120
	Precipitation (mm)	203.8	76.1	384.9	103.7	768.5

2.2. Measurements

This study divided the research region into three spatial scales: 1 km grid scale, county scale, and city scale. The 1 km grid scale was generated using the "Create Fishnet" function in ArcGIS 10.8. The study area data at the county scale and city scale units were extracted from the corresponding administrative boundary maps.

Groundwater monitoring was conducted from May 2021 through October 2022 at approximately 15–20-day intervals. Groundwater burial depth is measured using a portable groundwater meter (SWJ-90, Jinshui Huayu Information Technology Co., Ltd., Shandong, China), and mineralization is determined using an HQ30d portable multi-parameter water quality analyzer.

The soil water content (SWC), soil salt concentrations (SSC), yield, and quality were measured in the experimental field. In the three years, soil in the 0–100 cm layer was sampled at 20 cm increments every 2–3 days after irrigation in each biological replicate plot using a soil auger. Soil water content was measured by gravimetric method and converted

to volumetric water content with the bulk density. SSC was determined by the oven-drying residue method from the 1:5 extract. The electrical conductivity ($EC_{1:5}$) and saturated paste extract electrical conductivities (EC_e) were determined according to Bao [26] and Rhoades [27], respectively. The $EC_{1:5}$ of the 1:5 soil water extract was measured by a multi-parameter water quality instrument. The $EC_{1:5}$ (uS·cm^{-1}) is converted to the SSC (%) and EC_e, (dS·m^{-1}) with the following equation:

$$\text{SSC} = 2.5EC_{1:5} - 0.0427,\ EC_e = 2.46 + 3.03\frac{1.4}{0.431}EC_{1:5} \quad (1)$$

The rate of change of soil salinity (S_t) was calculated by comparing the difference between the final soil salt concentrations and the initial soil salt content, relative to the initial value, and expressed as a percentage.

Reference crop evapotranspiration (ET_0) was calculated using the FAO56 Penman-Monteith equation [28].

$$ET_0 = \frac{0.408\Delta(R_n - G) + \gamma\frac{900}{T+273}\mu_2(e_s - e_a)}{\Delta + \gamma(1 + 0.34\mu_2)} \quad (2)$$

where R_n is net radiation (MJ·m^{-2}·day^{-1}), G is the soil heat flux density (MJ·m^{-2}·day^{-1}), γ is a psychrometric constant (kPa·°C^{-1}), T is the air temperature at a 2 m height (°C), μ_2 is the wind speed at a 2 m height (m·s^{-1}), e_s is the saturation vapor pressure (kPa·°C^{-1}), e_a is the actual air vapor pressure (kPa·°C^{-1}), and Δ is the slope of the vapor pressure curve (kPa·°C^{-1}).

Potential crop evapotranspiration (ET_p) was determined by multiplying ET_0 by the crop coefficient (K_c) obtained using the dual Kc method [28]:

$$ET_p = K_c \cdot ET_0 \quad (3)$$

where K_c is the crop coefficient, the values of *Ziziphus jujuba* 'Dongzao' at different growth stages (leaf expansion stage, flowering and fruiting stage, fruit swelling stage, and maturity stage) were obtained using the K_c values obtained by Wei et al. [29], with values of 0.45, 0.63, 1.12 and 0.80, respectively.

Meteorological data, including air humidity, air temperature, rainfall, solar radiation, atmospheric pressure, and wind speed at a 2 m height, were collected using the Zhanhua and Wudi station on meteorological-data-sharing service network of the National Meteorological Administration of China (https://data.cma.cn/).

The relative yield (Y_r) was obtained as the ratio of actual total yield and maximum total yield for each cultivar. The relationship between irrigation water mineralization and relative yield was developed [30]:

$$Y_r = 100 - K(C - T) \quad (4)$$

where T is the mineralization threshold (g·L^{-1}), and K is the percentage decrease in yield due to an increase in mineralization per unit.

Similarly, the relationship between the EC_e and Y_r was calculated as follows [31]:

$$Y_r = \frac{Y_m}{1 + \left(\frac{C}{C_{50}}\right)^p} \quad (5)$$

where Y_m is the theoretical maximum yield, C_{50} is the salinity (dS·m^{-1}) that reduces the yield by 50%, and p is an empirical constant.

Within each replicate, 12 fruits were randomly harvested from multiple jujube trees. Fruits were collected from four directions and three canopy positions (upper, middle, and

lower) of the tree. The fruit shape index and single fruit weight were investigated by a vernier caliper (DL91150, DELI, Ningbo, China) and analytical balance (AR1502CN, OHAUS International Trading (Shanghai) Co., Ltd., Shanghai, China). Soluble sugar was measured by anthrone sulfuric acid colorimetry. The total soluble solid content of each fruit was measured using a digital refractometer (PAL-1, ATAGO Co., Ltd., Tokyo, Japan). Titratable acidity was determined using a modified titration method [32]. Vitamin C was determined by using 2, 6-dichlorophenol-indophenol titrimetric method.

2.3. Model Description

2.3.1. MODFLOW Model

Visual MODFLOW is based on the finite difference method and has been used extensively to simulate flow and transport processes in aquifer systems. The governing partial differential equation for a confined aquifer used in Visual MODFLOW is as follows:

$$\frac{\partial}{\partial x}\left(K_{xx}\frac{\partial h}{\partial x}\right)+\frac{\partial}{\partial y}\left(K_{yy}\frac{\partial h}{\partial y}\right)+\frac{\partial}{\partial z}\left(K_{zz}\frac{\partial h}{\partial z}\right)-W = S_y\frac{\partial h}{\partial t} \quad (6)$$

where K_{xx}, K_{yy}, and K_{zz} are the permeability coefficients of the aquifer along the x, y, and z coordinate directions, respectively ($m{\cdot}d^{-1}$); h is the head of the aquifer (m); W is the volumetric flux per unit volume, which represents pumping, recharge, or other sources and sinks (d^{-1}); S_y is the degree of gravity feed to the aquifer (m^{-1}); t is the time; and $\partial h/\partial t$ is the rate of change of the head with time ($m{\cdot}d^{-1}$).

In this study, according to the size and lithology of the area, the study area is divided into Area I and Area II, vertically divided into one layer, with the elevation of the shallow aquifer fixed at 30 m. The boundary conditions and the division of the area are shown in Figure 3. The upper boundary was defined by a recharge conditions condition. The lower boundary was conceptualized as a zero-flow boundary due to the poor soil permeability below 30 cm depth that restricts downward groundwater movement. The regional groundwater flow direction in the study area generally follows a south–north orientation, allowing the southern and northern boundaries to be conceptualized as discharge boundaries. The eastern and western boundaries were treated as no-flow boundaries given that the adjacent lands on both sides were hydraulically connected by drainage ditches and share the same village land use, resulting in negligible groundwater flux across the boundary.

2.3.2. HYDRUS Model

The HYDRUS model was used to simulate the movement of water and soluble salts in the soil–plant system under various irrigation management systems [33]. The Richards equation and the convection-dispersion equation were used to solve water flow and solute transport in the model, respectively:

$$\frac{\partial}{\partial x}\left(K(h)\frac{\partial h}{\partial x}\right)+\frac{\partial}{\partial z}\left(K(h)\frac{\partial h}{\partial z}\right)+\frac{\partial K(h)}{\partial z}-S(h) = \frac{\partial \theta(h)}{\partial t} \quad (7)$$

$$\frac{\partial}{\partial x}\left(\theta D_T\frac{\partial c}{\partial x}\right)+\frac{\partial}{\partial z}\left(\theta D_L\frac{\partial h}{\partial z}\right)-\frac{\partial (q_i c)}{\partial z}-S(h) = \frac{\partial(\theta c)}{\partial t} \quad (8)$$

where x and z are horizontal and vertical spatial coordinates (cm); θ is the volumetric soil water content ($cm^3{\cdot}cm^{-3}$); h the soil pressure head (cm); t is time (d); $K(h)$ is the unsaturated soil hydraulic conductivity ($cm{\cdot}d^{-1}$); $S(h)$ is the root water uptake (d^{-1}); c is the soil solution salt concentration ($g{\cdot}cm^{-3}$); q_i is the water flux ($cm{\cdot}d^{-1}$); D_T is the transverse dispersion coefficient ($cm^2{\cdot}d^{-1}$); D_L is the longitudinal dispersion coefficient ($cm^2{\cdot}d^{-1}$); and $S(h)$ is the source–sink term ($cm^3{\cdot}(cm^3{\cdot}d)^{-1}$), which here represents the root water uptake.

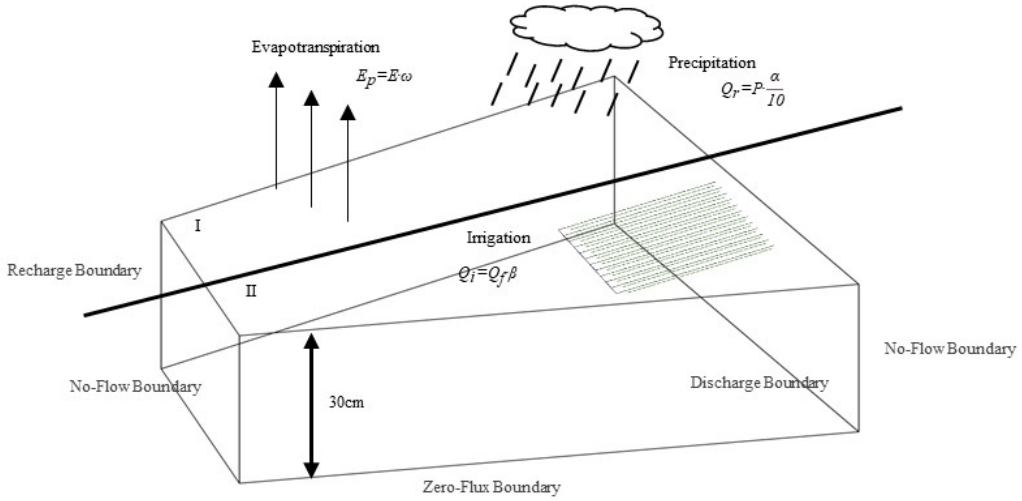


Figure 3. Schematic diagram of MODFLOW model boundary conditions and region division. Note: Q_r is the intensity of rainfall infiltration recharge in the study area (mm·y^{-1}); P is the multi-year average rainfall (mm); Q_i is the irrigation regression volume (m^3); Q_f is the irrigation volume of farmland (m^3); E_p is the intensity of submerged aquifer evapotranspiration (mm·y^{-1}); E is the multi-year average evapotranspiration on the water surface (mm); α is the coefficient of rainfall infiltration (dimensionless); β is the irrigation regression coefficient (dimensionless); and ω is the submersible evapotranspiration coefficient (dimensionless).

The soil hydraulic functions $\theta(h)$ and $K(h)$ in Equation (7) were described using the van Genuchten-Mualem model [31]:

$$\theta(h) = \theta_r + \frac{\theta_s - \theta_r}{\left[1 + |\alpha h|^n\right]^m} \tag{9}$$

$$K(h) = K_s S_e^l \left[1 - \left(1 - S_e^{\frac{1}{m}}\right)^m\right]^2,\ m = 1 - \frac{1}{n} \tag{10}$$

where θ_r is the residual moisture content of soil; θ_s is the saturated moisture content of soil; α, m and n are the shape coefficient of soil water characteristic curve; K_s is the saturated water conductivity; l is the pore connectivity parameter; and S_e is the dimensionless relative saturation factor.

Solute transport is described using the convection-dispersion equation:

$$\frac{\partial}{\partial x}\left(\theta D_T \frac{\partial c}{\partial x}\right) + \frac{\partial}{\partial z}\left(\theta D_L \frac{\partial h}{\partial z}\right) - \frac{\partial (q_i c)}{\partial z} - S(h) = \frac{\partial (\theta c)}{\partial t} \tag{11}$$

where c is the soil solution salt concentration (g·cm^{-3}); q_i is the water flux (cm·d^{-1}); D_T is the transverse dispersion coefficient (cm^2·d^{-1}); D_L is the longitudinal dispersion coefficient (cm^2·d^{-1}); and $S(h)$ is the source–sink term (cm^3·(cm^3·d)$^{-1}$), which, here, represents the root water absorption rate.

Root water uptake in Equation (12) was computed using the Feddes model [34] that considers water and salinity stresses simultaneously:

$$S(h) = \alpha(h) b(x,z) T_p L \tag{12}$$

$$\alpha(h) = \begin{cases} \frac{h_1 - h}{h_1 - h_2} & h_2 < h \le h_1 \\ 1 & h_2 \le h \le h_1 \\ \frac{h - h_4}{h_2 - h_4} & h_4 \le h < h_3 \end{cases} \tag{13}$$

where $\alpha(h)$ is the water stress coefficient; $b(x,z)$ is the root water uptake distribution density function, determined according to the actual root distribution; T_p is the potential transpiration rate (cm·d^{-1}); L is the maximum soil surface width of the root-zone distribution (cm);

and h_1, h_2, h_3, and h_4 are the different pressure heads of the root system for water uptake from the soil (cm).

A two-dimensional area 350 cm deep and 20 cm wide was defined as the modeling domain. Four boundary conditions were defined, i.e., the upper boundary, the bottom boundary, the left lateral boundary, and the right lateral boundary. The soil profile was divided into four soil layers of 0–20 cm (I), 20–80 cm (II), 80–100 cm (III), and 100–350 cm (IV) according to the soil texture, and the boundary conditions and area divisions are shown in Figure 4. The upper boundary was defined by an atmospheric boundary condition, incorporating specified rainfall and potential evaporation fluxes. Potential transpiration was applied across the entire surface boundary and subsequently distributed within the root zone according to the normalized root density profile. A time-variable head boundary condition, representing fluctuating shallow groundwater head, was implemented at the lower boundary. Both lateral boundaries were treated as no-flow boundaries. For solute transport, third-type (Cauchy) boundary conditions were applied at both the upper, and a time-dependent concentration boundary condition was adopted at the lower boundary.

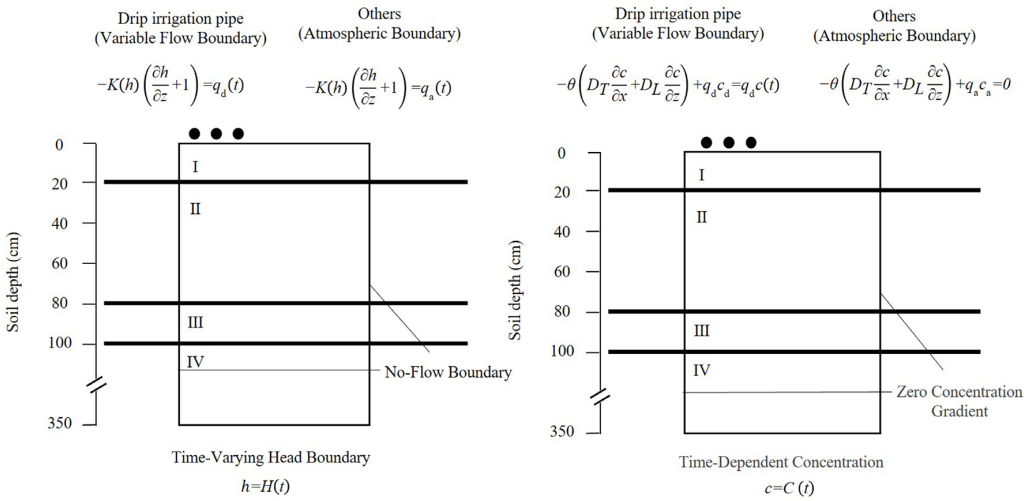


Figure 4. Schematic diagram of region division and boundary condition settings for the HYDRUS model: (**a**) moisture boundary; (**b**) solute boundary. Note: In the figure, $q_d(t)$ is the water flux from drip emitters ($cm \cdot d^{-1}$); $q_a(t)$ isthe atmospheric water flux (evaporation/precipitation) ($cm \cdot d^{-1}$); c_d is theirrigation water salinity ($g \cdot cm^{-3}$); $c(t)$ is the soil solution salt concentration ($g \cdot cm^{-3}$); c_a is the atmospheric solute concentration ($g \cdot cm^{-3}$); H is the pressure head converted from the measured groundwater depth (cm); C is the groundwater salinity ($g \cdot cm^{-3}$).

2.3.3. Coupling Scheme and Performance Evaluation of MODFLOW and HYDRUS-2D

One-way coupling was implemented between MODFLOW and HYDRUS-2D. The MODFLOW model adopted a single aquifer layer and simulated groundwater head fluctuations at the experimental plot. The time series of simulated groundwater heads were extracted and applied to the bottom boundary of the HYDRUS-2D domain (350 cm depth) as a time-variable pressure head boundary. At each computational time step, the bottom pressure head in HYDRUS-2D was updated using the groundwater head predicted by MODFLOW. This boundary condition dynamically controlled capillary rise or deep percolation at the base of the soil profile. No feedback from HYDRUS-2D to MODFLOW was considered in this coupling scheme.

The agreement and bias between simulated and observed values of SWC and SSC were quantitatively assessed using two statistical metrics: the coefficient of determination (r^2) and the root mean square error (RMSE). The calculation formulae were as follows:

$$r^2 = \left[\frac{\sum_{i=1}^{n} (S_i - S_{avr})(O_i - O_{avr})}{\sqrt{\sum_{i=1}^{n} (S_i - S_{avr})^2 \sum_{i=1}^{n} (O_i - O_{avr})^2}} \right]^2 \quad (14)$$

$$\text{RMSE} = \sqrt{\frac{1}{n} \sum_{i=1}^{n} (S_i - O_i)^2} \quad (15)$$

where we consider that O_i and S_i are the observed and simulated values; and O_{avr} and S_{avr} are the average of measured and predicted values at total n number of observed and simulated values, respectively.

2.4. Evaluating the Appropriate Long-Term Irrigation Schemes

This study first evaluates the resource guarantee, soil salt accumulation and crop yield reduction induced by shallow saline groundwater exploitation from regional and long-term dynamic perspectives, carries out a three-year field experiment with slightly saline water irrigation of different mineralization levels, collects basic data to establish and validate MODFLOW and HYDRUS-2D models, performs multi-scenario simulations under wet, normal and dry years based on 10-year climate data, analyzes the spatiotemporal variations of soil water and salt, as well as crop yield responses, and, finally, determines appropriate long-term saline water irrigation schemes balancing crop yield and soil salt accumulation control. Overall, the detailed flow chart is shown in Figure 5.

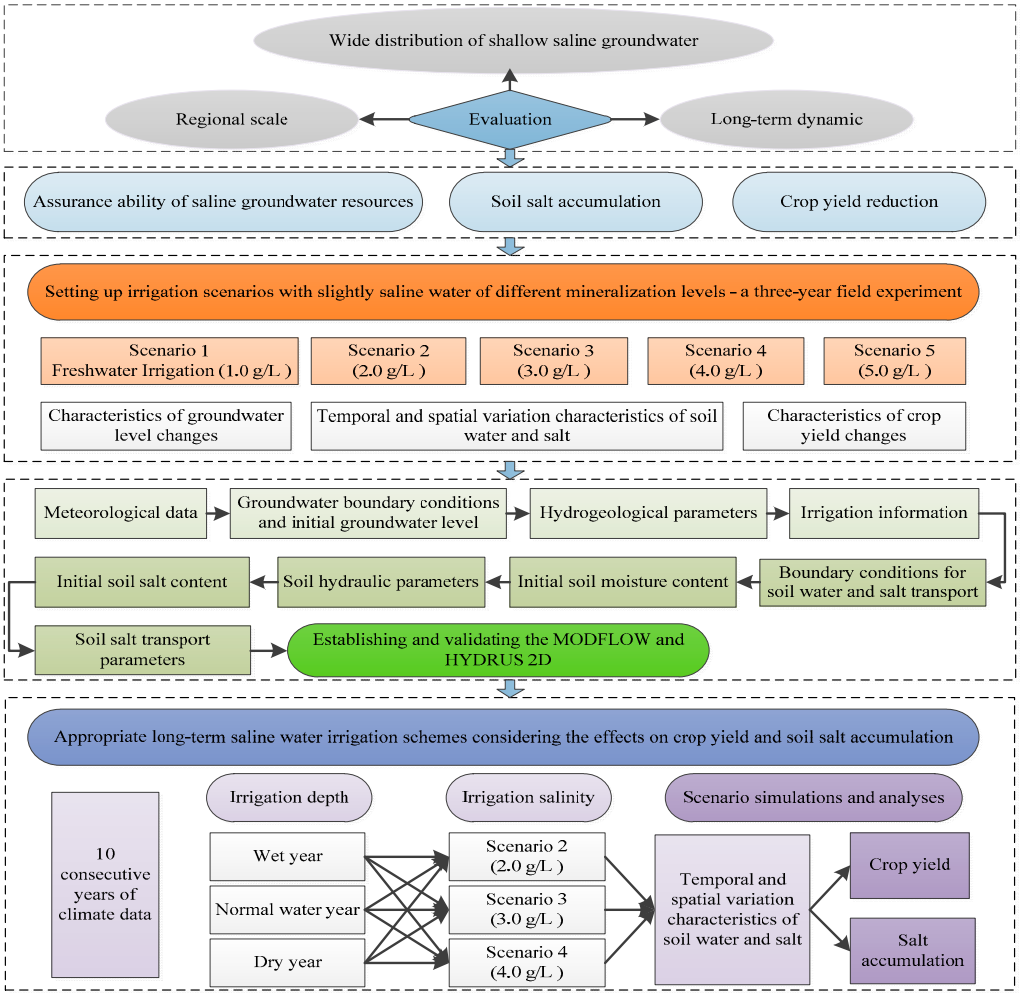


Figure 5. Technical flow of this study.

3. Experimental Results and Validation

3.1. Crop Yield and Quality

Crop yield is a key indicator for evaluating irrigation strategies [35]. Two sets of salt-tolerance indices were adopted in this study. The root-zone salinity thresholds were calculated using the Mass–Hoffman and van Genuchten salt-yield response functions, which take profile-weighted root-zone saturated paste electrical conductivity as the stress variable to characterize the inherent salt stress imposed by soil salinity on jujube roots. Under the brackish water drip irrigation mode with shallow groundwater in the study area, irrigation water salinity can directly induce salt stress on plants. To support field irrigation management, we further fitted the relationship between relative yield and irrigation water mineralization and obtained the annual irrigation salinity thresholds. The EC_e thresholds represent soil-derived salt stress for mechanistic analysis, while the irrigation water mineralization thresholds serve as practical references for brackish irrigation regulation. Figure 6a depicts the relationship between relative yield and the average root-zone electrical conductivity (EC_e) during the reproductive period. The crop salt-tolerance function indicates a salinity threshold of 4.51 dS·m^{-1} (0.087%) for jujube. The model further showed that EC_e values corresponding to relative yields of 85% and 50% were 8.85 dS·m^{-1} (0.19%) and 12.64 dS·m^{-1} (0.27%), respectively. Figure 6b illustrates the relationship between the relative yield of jujube and irrigation water salinity. The results indicate that the jujube relative yield decreased with increasing irrigation salinity, falling below 85% in both 2020 and 2022 when salinity exceeded 4 g·L^{-1}. Based on the Mass–Hoff crop salt-tolerance model, the irrigation salinity thresholds were determined as 1.05 g·L^{-1} (2020), 1.31 g·L^{-1} (2021), and 1.01 g·L^{-1} (2022).

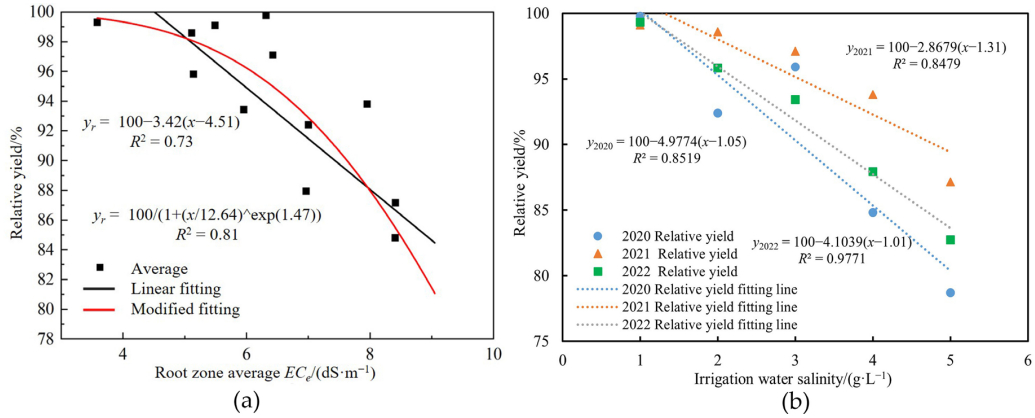


Figure 6. Relative yield of jujube in response to different root-zone EC_e (**a**) and irrigation mineralization (**b**).

In response to increasing irrigation water salinity, the comprehensive quality indicators of *Ziziphus jujuba* 'Dongzao' showed an initial improvement, followed by a decline (Table 3). There were no significant differences in fruit shape index among different treatments across the years ($p > 0.05$). Salinity treatment had a significant impact on single fruit weight ($p < 0.05$). Compared to 1 g·L^{-1}, the single fruit weight decreased by 10.87%, 20.35%, 8.62%, 15.48%, 5.76%, 32.58% in 4 g·L^{-1} and 5 g·L^{-1} treatments, respectively, over the three years. Although salinity levels of 4–5 g·L^{-1} significantly reduced individual fruit weight, the 3–5 g·L^{-1} range substantially enhanced key quality parameters including total soluble solids, titratable acid, and vitamin C content. These results indicate that mild saline water irrigation (2–4 g·L^{-1}) can effectively improve specific fruit quality attributes, with peak enhancement occurring at 4 g·L^{-1}.

Table 3. Effects of the salinity of irrigation water on quality indices of *Ziziphus jujuba* 'Dongzao'.

Year	Salinity/(g·L^{-1})	Fruit Shape Index	Single Fruit Weight/g	Soluble Sugar/%	Total Soluble Solids/%	Titratable Acid/%	Vitamin C/(mg·g^{-1})
2020	1	0.95 ± 0.04 a	24.57 ± 1.77 a	19.78 ± 0.20 c	21.10 ± 0.75 b	0.12 ± 0.01 b	2.82 ± 0.16 c
	2	1.01 ± 0.01 a	22.99 ± 0.59 a	20.26 ± 0.20 b	22.27 ± 0.68 a	0.12 ± 0.01 b	2.93 ± 0.14 b
	3	1.01 ± 0.02 a	23.99 ± 0.40 a	21.68 ± 0.20 b	23.70 ± 1.73 a	0.16 ± 0.01 a	3.12 ± 0.08 b
	4	1.01 ± 0.01 a	21.90 ± 0.68 b	22.34 ± 0.20 a	24.23 ± 0.30 a	0.16 ± 0.01 a	3.65 ± 0.06 a
	5	0.98 ± 0.02 a	19.57 ± 2.12 b	20.72 ± 0.20 b	22.13 ± 0.80 a	0.14 ± 0.01 ab	3.07 ± 0.13 b
2021	1	0.97 ± 0.01 a	23.78 ± 1.89 a	17.06 ± 0.50 a	20.07 ± 1.36 b	0.29 ± 0.01 b	2.41 ± 0.04 b
	2	0.98 ± 0.01 a	24.16 ± 2.77 a	16.59 ± 0.57 a	21.42 ± 0.89 b	0.27 ± 0.02 b	2.53 ± 0.16 a
	3	0.96 ± 0.07 a	23.79 ± 2.45 a	17.47 ± 0.98 a	21.27 ± 0.92 b	0.32 ± 0.01 a	2.60 ± 0.20 a
	4	0.99 ± 0.05 a	21.73 ± 1.91 b	19.18 ± 1.24 a	22.89 ± 0.59 b	0.32 ± 0.02 a	2.62 ± 0.18 a
	5	0.98 ± 0.05 a	20.10 ± 3.07 b	18.05 ± 0.3 a	24.18 ± 1.03 a	0.34 ± 0.03 a	2.51 ± 0.05 a
2022	1	0.96 ± 0.11 a	15.44 ± 1.44 a	17.06 ± 0.50 a	20.07 ± 1.36 b	0.22 ± 0.02 b	2.41 ± 0.04 b
	2	0.92 ± 0.06 a	17.56 ± 1.52 a	16.59 ± 0.57 a	21.42 ± 0.89 b	0.26 ± 0.02 b	2.53 ± 0.16 a
	3	1.01 ± 0.10 a	18.31 ± 1.56 a	17.47 ± 0.98 a	21.27 ± 0.92 b	0.29 ± 0.03 a	2.60 ± 0.20 a
	4	1.04 ± 0.08 a	14.55 ± 1.56 b	19.18 ± 1.24 a	22.89 ± 0.59 b	0.36 ± 0.02 a	2.62 ± 0.18 a
	5	0.98 ± 0.09 a	10.41 ± 2.81 c	18.05 ± 0.3 a	24.18 ± 1.03 a	0.33 ± 0.03 a	2.51 ± 0.05 a

Note: Different letters in the same column indicate significant differences in the treatment of the same parameter ($p < 0.05$).

3.2. Model Validation

3.2.1. Simulation of Groundwater Head

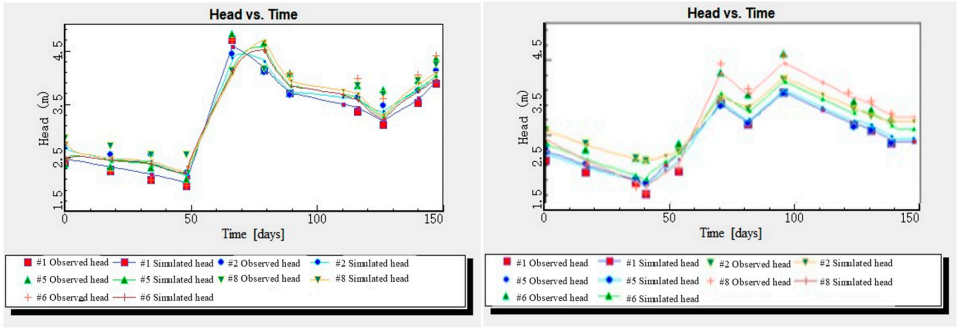
Based on the hydrogeological conditions of the study area and previous relevant studies, initial hydrogeological parameters were assigned to the two subzones of the MODFLOW model. Groundwater level data collected from five observation wells during 2021–2022 were used to calibrate and validate the groundwater flow model. Hydraulic conductivity in the x-, y-, and z-directions (K_x, K_y, and K_z, respectively) describes the ability of the aquifer to transmit groundwater along different directions, whereas the specific yield (S_y) represents the volume of water released from storage per unit horizontal area of an unconfined aquifer per unit decline in the water table [36]. These parameters govern groundwater flow and storage responses and, therefore, influence the simulated spatial distribution and temporal fluctuations of groundwater heads [37]. The final calibrated parameter values for the two subzones are presented in Table 4.

Table 4. Rate values of groundwater numerical model parameters.

Parameters/Partitions	K_x/(cm·s^{-1})	K_y/(cm·s^{-1})	K_z/(cm·s^{-1})	S_y
I	9×10^{-5}	9×10^{-5}	9×10^{-6}	0.025
II	8×10^{-4}	8×10^{-4}	8×10^{-5}	0.03

Figure 7 illustrates the relationship between observed and simulated groundwater heads at five monitoring wells during the calibration and validation periods. The simulated groundwater levels agree well with the field observations, demonstrating that the model can satisfactorily reproduce the dynamic variations in the groundwater regime under irrigation conditions (Table 5). As shown in Table 5, the Root Mean Squared values were 0.244 m and 0.111 m, while the Normalized RMS values were 8.582% and 5.891% during the calibration and validation periods, respectively. According to the groundwater modeling guidelines, Normalized RMS values below 10% generally indicate a good fit, although the acceptability of the model performance should also be considered in relation to the model objectives and hydrogeological conditions [38]. The correlation coefficients were 0.965 and 0.973 during the calibration and validation periods, respectively, indicating strong positive linear relationships between the observed and simulated groundwater heads. However,

correlation coefficients alone cannot fully reflect the magnitude of simulation errors. Taken together, these indicators suggest that the MODFLOW model reproduced groundwater head variations with reasonable accuracy during both periods.



(**a**) Calibration period (**b**) Validation period

Figure 7. Plot of the results of fitting the calculated and observed groundwater head values for the calibration period (**a**) and the validation period (**b**).

Table 5. The results of the statistical evaluation of the models for simulating groundwater heads.

Parameter	Standard Error of the Estimate (m)	Root Mean Squared (m)	Normalized RMS (%)	Correlation Coefficient
Calibration	0.009	0.244	8.582	0.965
Validation	0.004	0.111	5.891	0.973

3.2.2. Simulation of Soil Water Content and Salinity

Soil hydraulic parameters were initially estimated using the Rosetta Lite V1.1 program based on soil texture and bulk density data. Initial solute transport parameters, including the bulk density (γ_d), molecular diffusion coefficient in free water (*Fract*), and molecular diffusion coefficient in soil air (*ThImob*), were determined according to the experimental area's soil texture, following established methods [39]. The Feddes model simulated root water uptake reduction due to soil water stress. Water stress response parameters were adopted from the literature [40]. Salinity stress effects on root water uptake were simulated using a threshold value (1.5 g·kg^{-1}) and linear slope (14%) based on Karandish and Simůnek [41]. HYDRUS simulations employed the calibrated soil hydraulic and solute transport parameters from Table 6.

Table 6. Input values and calibrated coefficient in HYDRUS model.

Depth /cm	θ_r /(cm^3·cm^{-3})	θ_s /(cm^3·cm^{-3})	α /(cm^{-1})	n	K_s /(cm·d^{-1})	l	γ_d /(g·cm^{-3})	D_L /cm	D_T /cm	D_w /(cm^2·d^{-1})	D_p /(cm^2·d^{-1})
0–20	0.074	0.437	0.006	1.633	15.86	0.5	1.3	10	1	1	0
20–80	0.054	0.326	0.076	1.842	20.89	0.5	1.4	5	0.5	1	0
80–100	0.074	0.433	0.006	1.630	14.06	0.5	1.5	10	1	1	0
100–350	0.067	0.45	0.020	1.410	10.80	0.5	1.5	5	0.5	1	0

Note: θ_r is the residual moisture content of soil; θ_s is the saturated moisture content of soil; α and n are the shape coefficient of soil water characteristic curve; K_s is the saturated water conductivity; l is the pore connectivity parameter. γ_d is bulk density; D_L is longitudinal dispersion; D_T is lateral dispersion; D_w is molecular diffusion coefficient in free water; and D_p is soil gas diffusion coefficient.

Model calibration utilized the observed soil water contents and salt concentrations measurements across multiple monitoring points. The performance of the HYDRUS-2D model was evaluated by comparing the simulated and observed soil water content (SWC) and soil salt concentration (SSC) at different soil depths. Figure 8 compares the observed

and simulated soil water content distributions (a,b) and salt concentration distributions (c,d) at various depths under 3 g·L^{-1} irrigation.

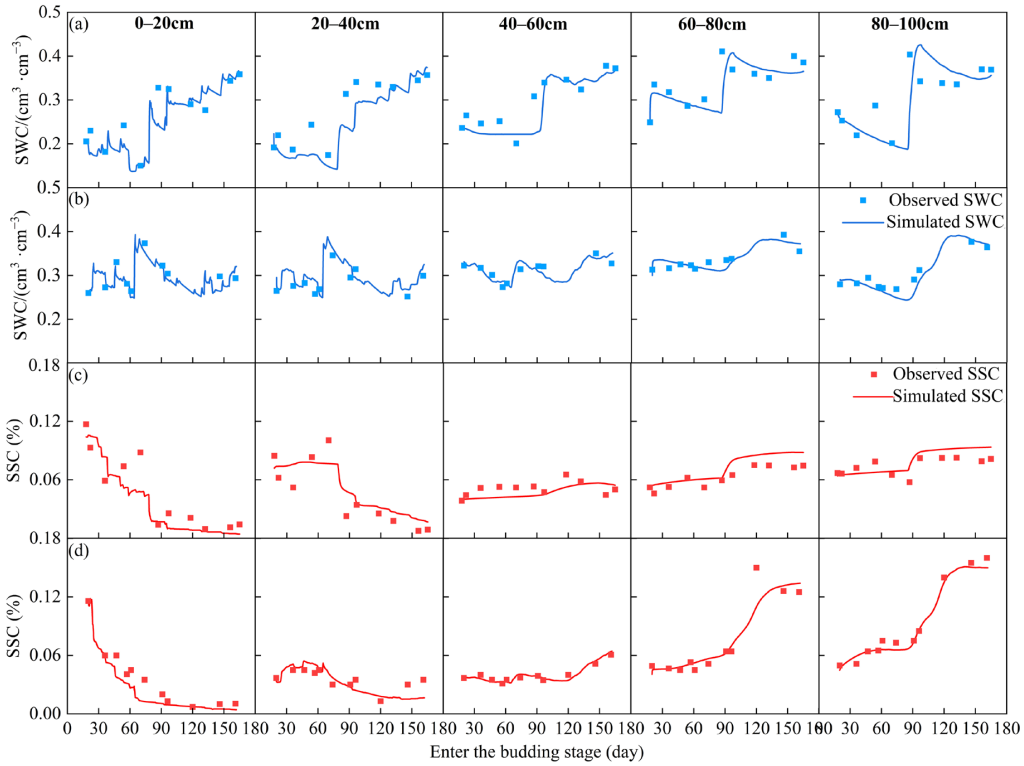


Figure 8. The comparison of the observed and simulated soil water content and salt concentration at different depths under 3 g·L^{-1} saline water irrigation: (**a**) calibration SWC; (**b**) validation SWC; (**c**) calibration SSC; (**d**) validation SSC.

Generally, a good agreement exists between the observed and simulated water contents, though values in the upper soil layer (0–40 cm) were consistently lower than in deeper layers (40–100 cm) across all depths. This discrepancy likely stems from the differences between simulation assumptions and field conditions. Actual precipitation events occur rapidly, followed by intensive evaporation during immediate post-precipitation periods. Conversely, the model simplified precipitation as single-day events and constrained evaporation rates below potential levels. In addition, there was a phenomenon where the observed values were higher than the simulated values in the 60 cm soil layer. The reason for this phenomenon was analyzed to be that all calculations in the model were considered ideal, but, in reality, the root water absorption rate exceeded the model's expectations, and water moved downward under gravity, resulting in the measured values in the 80 cm soil layer being higher than the simulated values in the later stage. These modeling simplifications probably contribute to observed soil water content deviations. During the crop growth stages, the observed and simulated soil salt concentrations exhibited similar temporal variation patterns. It can be observed that the model simulation can effectively reproduce the observed soil salinity during the two winter jujube-growing seasons. In terms of the difference between the simulated and measured soil salt content values, in terms of time, during the simulation process, the salt concentrations in the upper layer of soil (0–40 cm) can be diluted by irrigation and precipitation, but increases continuously with transpiration and evaporation. The salt concentrations in the deeper soil (40–100 cm) gradually increase because its salt concentrations are less affected by irrigation, and the upward water flux continuously brings salt from the deeper soil into this layer, resulting in an increasing simulation error. Vertically, the error between the measured and simulated values of salt concentrations in each soil layer

during the two winter-jujube growing seasons is similar to the results of water simulation. The difference between the observed and simulated values in the upper layer is higher than that in the lower layer, but its simulation accuracy is lower than that of the soil volumetric moisture content simulation. The reason for this may be due to two aspects: Firstly, the spatiotemporal variability of soil salinity includes the transformation of soil minerals, plant absorption, and solute desorption, which makes the spatiotemporal variability of salinity significantly higher than that of moisture; and, secondly, salt is transported with water, and, in reality, the dispersion coefficient of salt transport is lower than that of water solute transport parameters.

To evaluate the model accuracy, two key statistical performance metrics, RMSE and r^2, were calculated by comparing the simulated and observed soil water content and soil salinity. The validation results showed considerable variation in HYDRUS-2D model performance across soil depths and irrigation treatments (Table 7). As shown in Table 7, for SWC during calibration, the r^2 values between simulated and observed values were all greater than 0.6 and the RMSE was below 0.05 $cm^3 \cdot cm^{-3}$. For the validation period, r^2 exceeded 0.6 for all layers except the 20–40 cm layer under treatment S2, with RMSE less than 0.05 $cm^3 \cdot cm^{-3}$. In general, r^2 increased and RMSE decreased with soil depth, indicating better model performance for deeper soil layers. For soil salt concentration, during calibration, r^{22} values were above 0.6 for most cases except the 40–60 cm layer of treatments S3 and S4, and RMSE was less than 6%. In the validation period, r^2 was greater than 0.6 for most treatments, with RMSE below 3%. Vertically, larger mismatches between simulations and observations occurred in the 20–60 cm layer. This layer is the main root zone of *Ziziphus jujuba* 'Dongzao', where the salt transformation and biogeochemical processes are complex. Specifically, S3 and S4 correspond to a critical mineralization range of brackish irrigation water. Unlike the low-salinity treatments S1 and S2, where salt transport is dominated by simple leaching, a moderate salt input in S3 and S4 triggers coupled non-linear processes in the root zone, including cation exchange, adsorption–desorption and mineral dissolution–precipitation. Salt stress also modifies the root water uptake and transpiration patterns of winter jujube. This explains the relatively low r^2 values (0.50–0.63) observed in certain treatments at this depth, while r^2 can reach up to 0.98 in other layers and treatments. Overall, the model achieved reliable simulations for soil water, whereas the predictive accuracy of soil salinity varied markedly with soil depth and irrigation regime. The relatively poor performance within the root zone is attributed to the complex salt transformation, root water uptake and spatial heterogeneity of soil properties. Therefore, the overall model performance should not be summarized as uniformly satisfactory; salinity predictions from low-r^2 zones need careful interpretation, especially when extrapolated to long-term irrigation scenarios.

Table 7. Statistical comparison of simulated and observed values.

Parameter		Depth (cm)	1 g·L^{-1}		2 g·L^{-1}		3 g·L^{-1}		4 g·L^{-1}		5 g·L^{-1}	
			r^2	RMSE (%)	r^2	RMSE (%)	r^2	RMSE (%)	r^2	RMSE (%)	r^2	RMSE (%)
Calibration	SWC	20	0.83	2.35	0.87	2.54	0.79	3.55	0.84	3.01	0.60	3.51
		40	0.87	3.44	0.80	3.38	0.81	3.89	0.87	3.58	0.77	3.50
		60	0.80	2.70	0.81	2.61	0.80	3.13	0.83	2.35	0.71	4.50
		80	0.88	2.00	0.77	2.99	0.79	2.12	0.89	1.85	0.67	3.26
		100	0.92	2.24	0.91	2.77	0.82	3.04	0.89	2.24	0.82	3.72
	SSC	20	0.57	2.23	0.77	1.95	0.83	3.01	0.86	2.19	0.85	2.09
		40	0.81	1.78	0.79	1.82	0.67	2.74	0.72	3.54	0.68	5.22
		60	0.75	1.89	0.61	1.90	0.53	3.10	0.58	1.89	0.66	2.35
		80	0.88	1.71	0.90	2.01	0.77	2.88	0.65	3.67	0.78	2.78
		100	0.96	1.32	0.92	4.51	0.79	3.21	0.71	3.80	0.79	2.33

Table 7. *Cont.*

Parameter		Depth (cm)	1 g·L^{-1}		2 g·L^{-1}		3 g·L^{-1}		4 g·L^{-1}		5 g·L^{-1}	
			r^2	RMSE (%)	r^2	RMSE (%)	r^2	RMSE (%)	r^2	RMSE (%)	r^2	RMSE (%)
Validation	SWC	20	0.82	2.06	0.70	1.88	0.61	2.19	0.75	2.13	0.63	1.56
		40	0.90	1.43	0.56	2.04	0.67	2.34	0.67	2.24	0.62	1.80
		60	0.80	2.36	0.60	1.76	0.64	1.40	0.78	1.14	0.62	2.08
		80	0.84	1.53	0.64	1.94	0.73	1.30	0.64	1.03	0.88	2.03
		100	0.89	1.74	0.97	1.38	0.91	1.62	0.82	1.77	0.91	1.52
	SSC	20	0.88	1.54	0.89	1.86	0.84	1.26	0.83	1.73	0.80	2.69
		40	0.58	1.59	0.86	1.83	0.62	0.97	0.79	2.86	0.77	2.99
		60	0.73	0.67	0.50	0.41	0.94	0.26	0.60	0.43	0.62	0.90
		80	0.92	0.54	0.97	0.05	0.98	0.56	0.95	0.39	0.82	1.11
		100	0.97	0.58	0.98	0.08	0.98	0.59	0.94	1.80	0.63	0.41

4. Discussion

4.1. Irrigation Scenario

To evaluate irrigation management practices for saline soils in this region, multi-year simulations (2010–2019) assessed water–salt balance responses to different irrigation salinities. Field experiments revealed that a consecutive 3-year application of 4–5 g·L^{-1} saline irrigation reduced jujube yields by >85%, while mild salinity (4 g·L^{-1}) optimally enhanced certain fruit quality attributes. Accordingly, the upper threshold of irrigation salinity for jujube was set as 4 g·L^{-1} in the scenario simulation. Three irrigation salinity levels (2, 3, and 4 g·L^{-1}) were simulated using calculated growing-season precipitation (p) for 25%, 50%, and 75% hydrologic years (585, 466, and 367 mm, respectively), reflecting the local hydrological variability. In this modelling framework, the single irrigation quota was fixed at 24 mm per irrigation event (fixed factor). The two independently controlled variables were irrigation water salinity and hydrological year type; irrigation frequency was determined dynamically by the crop water requirement minus effective rainfall and was not treated as an independent variable. The time-variable groundwater head boundary derived from MODFLOW was identical for all simulation runs to exclude confounding groundwater differences. The irrigation scheduling rules were as follows: In wet years ($p \geq 585$ mm), apply two to three irrigations from the leaf expansion stage to the flowering and fruiting stage (pre-flowering and fruit-setting water), with optional supplemental irrigation during the maturity stage; in normal years (466 mm $\leq p <$ 585 mm), irrigate three to four times during the early growth stages, plus one to two fruit-expansion irrigations and one to two coloring irrigations; under mild dry years (367 mm $\leq p <$ 466 mm), implement two pre-flowering, five to six fruit-setting/fruiting, and one to two coloring irrigations; during severe dry years ($p <$ 367 mm), increase to two pre-flowering, six to eight fruit-setting/fruiting, and one to two coloring irrigations, with adjustments permitted based on real-time rainfall and crop water requirements during the growth period. The detailed irrigation schedule is shown in Table 8. The initial and boundary conditions of all schedules were identical to those of the treatment in the experiment. The groundwater head in January 2020 and the soil water salt content in April 2020 were used as the initial values of the model. The irrigation dates were April 16th to May 25th, May 26th to June 25th, June 26th to August 31st and September 1st to 30th, respectively, in the germination to leaf expansion stage, flowering and fruiting stage, fruit swelling stage, and maturity stage. The simulation period covered from the emergence to harvest stages of jujube growth. Table 8 presents the monthly rainfall during the growth stages of winter jujube from 2010 to 2019, along with the irrigation timing and frequency determined based on rainfall distribution.

Table 8. Jujube-appropriate designing irrigation amounts at different growth stages.

Years	*p* During the Growing Period/mm						Irrigation Amount/mm						Annual	Hydrological
Month	4	5	6	7	8	9	4	5	6	7	8	9	*p*/mm	Year
2010	13.5	61.1	45.5	60.6	273.3	56.5	24	24	24	48	-	24	554.2 **	Normal water year
2011	26.4	39.4	38.4	140.0	228.5	66.5	24	24	24	24	-	24	623.3 **	Normal water year
2012	43.5	14.0	70.2	161.8	242.1	44.0	24	24	24	24	-	24	656.2 **	Normal water year
2013	26.9	42.4	41.0	384.0	72.9	18.6	24	24	24	-	48	48	652.2 **	Normal water year
2014	4.3	53.5	71.3	46.0	35.4	59.1	24	24	24	72	96	24	316.6 *	Dry year
2015	50.3	41.4	48.1	167.9	295.0	14.0	-	24	24	-	-	24	709.9 ***	Wet year
2016	13.7	47.7	155.3	204.7	240.3	34.0	24	24	24	-	-	-	770.2 ***	Wet year
2017	24.7	9.4	82.7	196.8	168.3	5.2	24	24	24	24	-	48	557.7 **	Normal water year
2018	39.6	99.7	161.7	251.2	315.6	23.6	-	24	24	-	-	-	913.1 ***	Wet year
2019	34.0	6.7	32.7	156.1	331.4	5.6	24	24	24	24	-	48	622.2 **	Normal water year

Note: *, **, and *** indicate dry, normal, and wet annual hydrological years, respectively.

4.2. Simulation of the Groundwater Head and Soil Water, and Salt Changes in the Soil Profiles

Under experimental irrigation scenarios, groundwater head fluctuations from 2010 to 2019 are presented in Figure 9. Simulated groundwater heads ranged from 1.53 to 4.43 m, peaking at 240 d (2010) and reaching minimum levels at 1560 d (2014). The results confirm precipitation as the dominant driver of groundwater dynamics, with a significantly enhanced recharge during wet years, causing pronounced water level rises compared to dry periods. During annual flood seasons (from June to September), more substantial head increases occurred due to frequent heavy rainfall events and reduced agricultural extraction, consistent with the regional recharge patterns reported by Zhang et al. [42]. This groundwater model simulated the water table as the lower boundary for soil water–salt transport, generating soil water content and salinity distributions from 15 April 2010 to 1 October 2019 across irrigation scenarios.

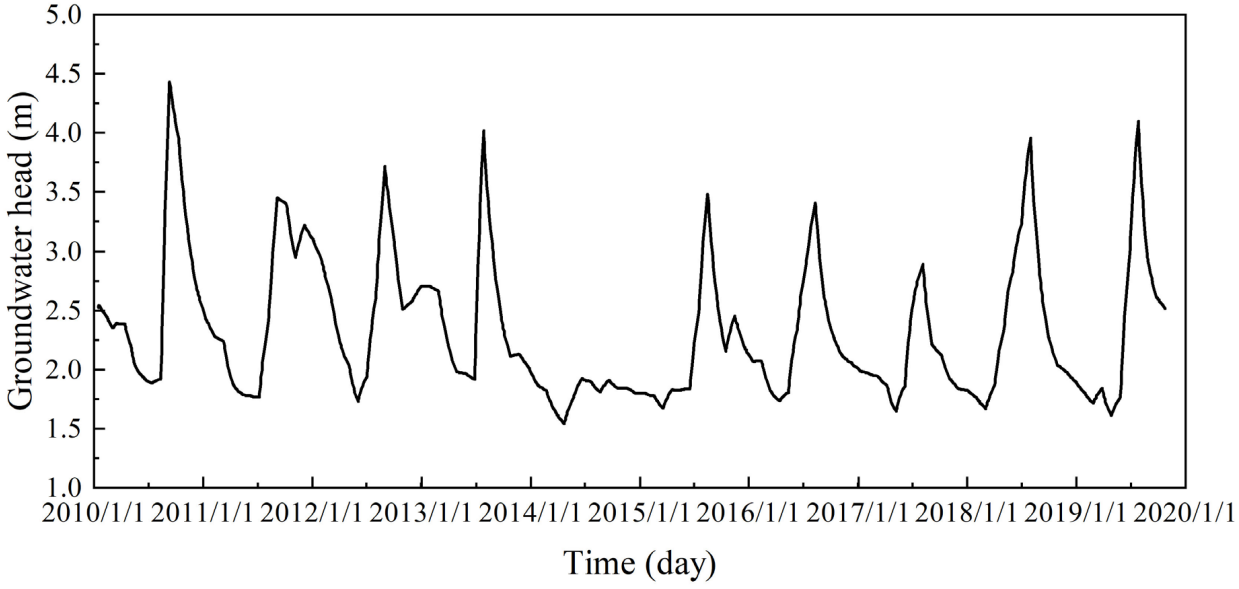


Figure 9. Simulation results of groundwater head from 2010 to 2019.

Figure 10 shows the simulated results of SWC and SSC in the 0–100 cm soil profile during 10 years of continuous irrigation with saline water. The SWC in the soil profile's upper layer (0–40cm) fluctuated but changed only slightly in the deeper layer (40–100 cm).

The SWC in the upper layers is mainly influenced by precipitation and evaporation. During drought years, the deeper-layer SWC is significantly affected by irrigation water salinity. The salt stress from high-salinity irrigation suppresses root water uptake, effectively reducing the plant's water consumption and leading to a higher residual moisture content in the soil. The range of SSC fluctuation dampens progressively with soil depth. While driven by the salinity of irrigation water, the SSC is further modulated by pronounced seasonal and yearly fluctuations, primarily governed by rainfall leaching. Salt accumulation occurred at the soil profile's depths of 40–60 cm, with a marked increase under the 4 g·L^{-1} irrigation treatment, where the SSC values increased from 0.09 to 0.33 cm^3·cm^{-3}.

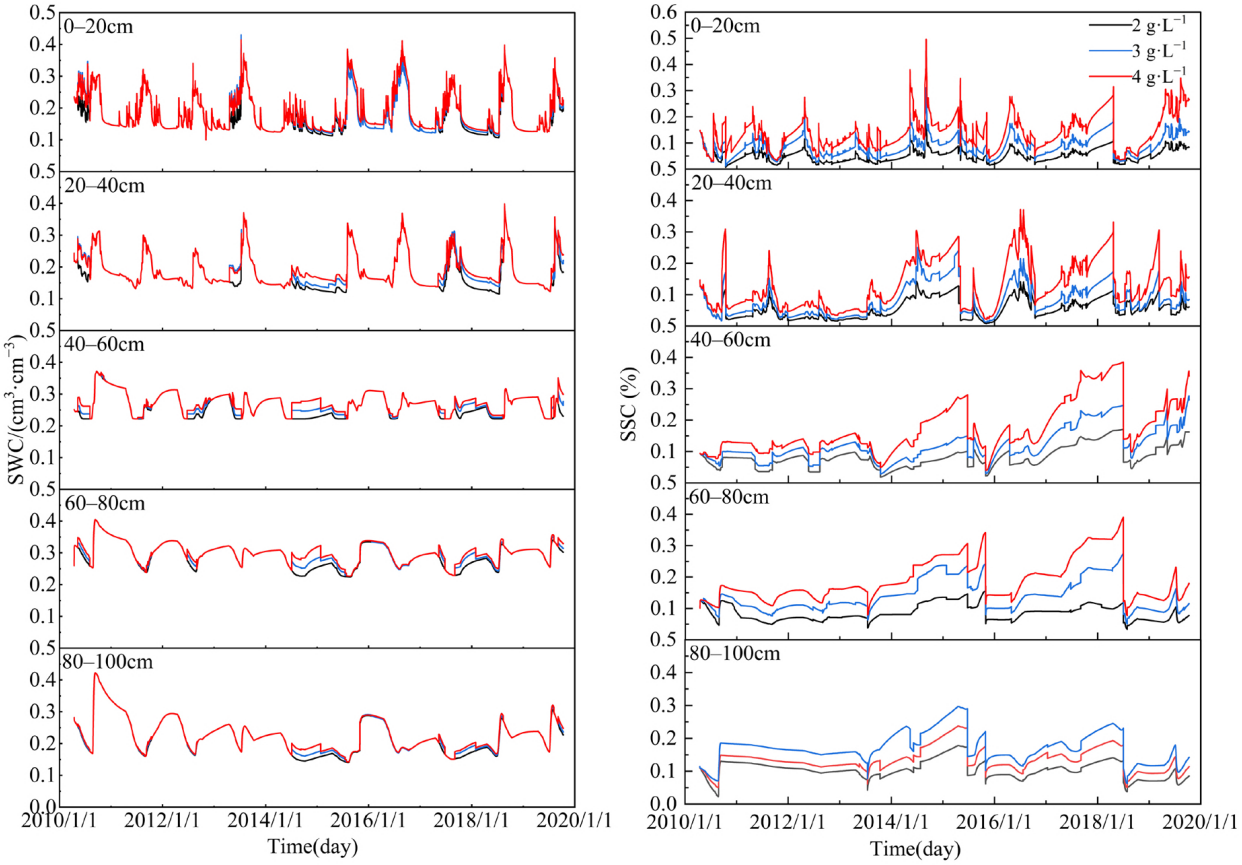


Figure 10. Simulation results of SWC and SSC changes under continuous irrigation with slightly saline water of different mineralization levels for 10 years.

4.3. Saline Water Drip Irrigation Strategies

Given the concentration of jujube roots within the 60 cm soil layer, Figure 11 presents the simulated soil water content (0–80 cm depth) across irrigation scenarios. The figure lists the optimal lower limits of soil moisture content for each phenological stage, which were determined with reference to the Technical Regulations for Irrigation and Drainage and Waterproofing of Jujube Orchards [43] developed by the Binzhou Forestry Society. Although the 2 g·L^{-1} treatments in 2015 and 2017 exhibited slightly suboptimal water content during the leaf expansion stage, all scenarios maintained adequate water availability for normal plant growth, as irrigation was triggered whenever the relative water content dropped below 45%. Simulations revealed that soil water content increased with irrigation salinity during critical stages (the flowering and fruiting stage), while non-drought periods showed negligible differences between salinity treatments. High-salinity irrigation-induced osmotic stress, reducing root-zone water potential gradients and inhibiting water uptake. However,

the model's uniform root water uptake parameters likely underestimated the salinity stress effects on the absorption capacity during non-drought periods [44].

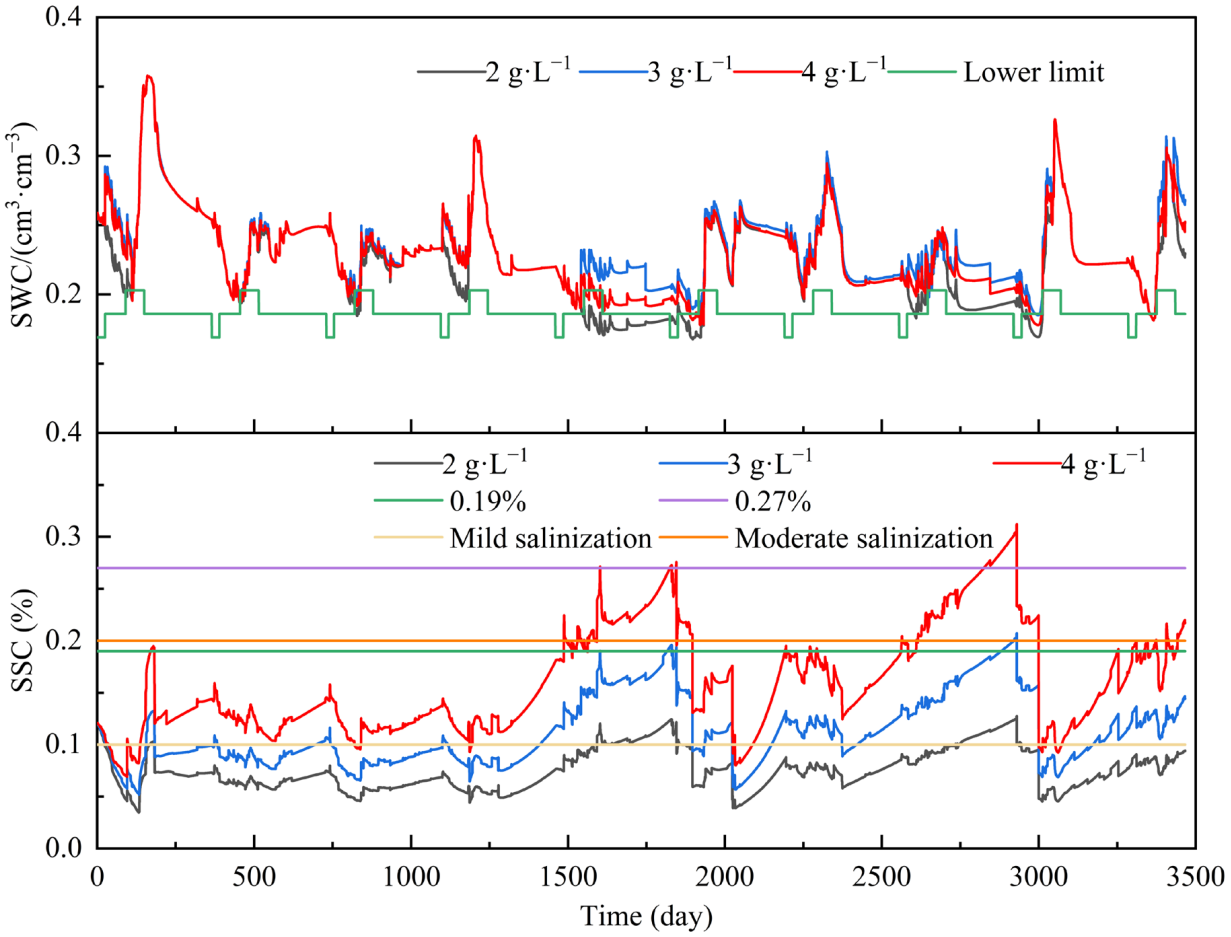


Figure 11. Simulation results of average soil water content (SWC) and salt concentration (SSC) from 0 to 100 cm for 10 years of continuous irrigation with saline water of different mineralization levels.

To safeguard the jujube yield and soil quality under varying salinity conditions, Figure 11 presents the simulated soil salinity dynamics (0–100 cm) across scenarios, annotated with key thresholds: 0.19% (85% relative yield) and 0.27% (50% relative yield) salinity levels, alongside slightly/moderately salinization classification standards. The results showed that there were significant differences in the effects of saline water with different mineralization levels on the salinity dynamics in the 0–100 cm soil layer of date fields under 10 years of continuous irrigation. Soil salinity in the 2 g·L^{-1} treatment was consistently maintained below 0.13%, and more than 85% of the time periods were kept at a safe level (<0.1%); the 3 g·L^{-1} treatment showed a transient increase in salinity only when the annual precipitation was <540 mm, but the time periods that exceeded the salinity tolerance threshold for jujube dates (0.19%) only accounted for 2% of the time periods; the 4 g·L^{-1} treatment showed the salt accumulation phenomenon in drought years (precipitation <540 mm); 32% of the time periods exceeded the 0.19% threshold. This shows that continuous irrigation using water at 2 g·L^{-1} and 3 g·L^{-1} salinity does not cause progressive accumulation of soil salinity over years, and soil salinity fluctuates dynamically below 0.2%. Nevertheless, when annual precipitation is less than about 540 mm, irrigation with 4 g·L^{-1} saline water restrains jujube growth and may trigger moderate soil salinization.

Figure 12 presents the interannual variations in salt accumulation rate and final salt content (0–100 cm) for *Ziziphus jujuba* 'Dongzao' after each growing season. All treatments

caused net salt accumulation except during the initial year when rainfall exceeded 623 mm, and for the 4 g·L^{-1} treatment in 2014. Salt accumulation rates generally increased with irrigation salinity. After 10 years, the 2 g·L^{-1} treatment reduced soil salinity by 22.21% versus initial levels, 3 g·L^{-1} increased salinity by 19.37%, and 4 g·L^{-1} increased salinity by 79.76%. Soil quality progressively declined with higher irrigation salinity, reaching moderate salinization under the 4 g·L^{-1} treatment. This pattern stems from the accumulation of soluble salts from saline water on soil colloids [45], where the greater salinity introduced more ions. Unlike the 2 and 3 g·L^{-1} treatments, the 4 g·L^{-1} treatment showed reduced salt accumulation in 2014 despite drought conditions. This anomaly resulted from elevated irrigation volumes enhancing leaching and deep salt displacement [46], which counteracted the salinity accumulation trends observed in other years.

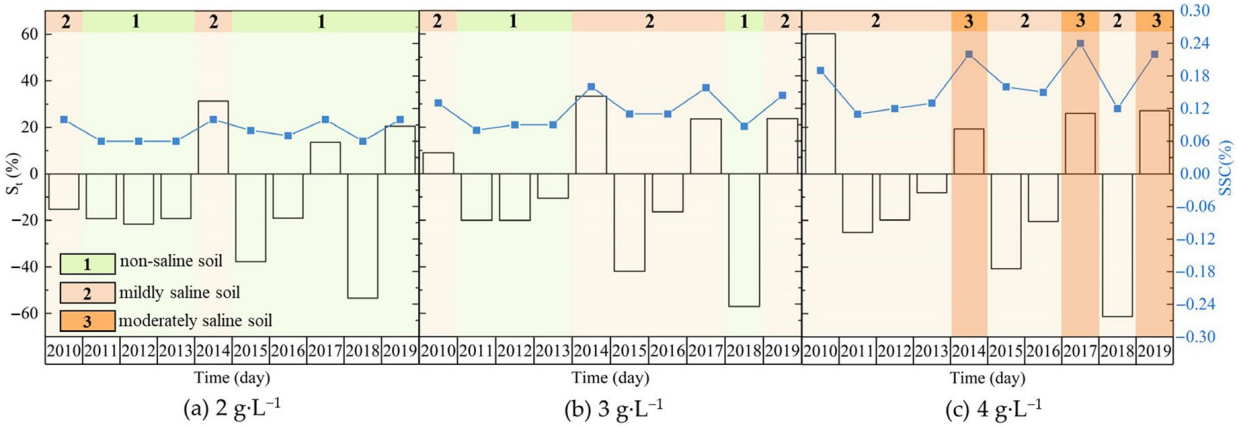


Figure 12. Analysis of soil environmental parameters under different irrigation water mineralization during the decade-long simulation: (**a**) 2 g·L^{-1}; (**b**) 3 g·L^{-1}; (**c**) 4 g·L^{-1}.

To ensure the sustainable development of the *Ziziphus jujuba* 'Dongzao' industry and maintain ecological balance, this study optimized saline drip irrigation strategies with dual objectives: preserving the soil–water environment and sustaining a relative yield of ≥85%. The experimental and simulation results identify 3 g·L^{-1} as the baseline irrigation salinity. Martínez-Moreno et al. [47] confirmed that a higher salinity level (4 g·L^{-1}) is viable in high-leaching soils to prevent short- to medium-term salt accumulation. Given that the leaching capacity is positively correlated with rainfall [48], we recommend the following: 4 g·L^{-1} in high-precipitation years and 2 g·L^{-1} in low-precipitation years. As prolonged saline irrigation requires temporal limits [49], alternating irrigation regimes—a well-established approach—can balance soil salinity during consecutive drought years or under high-salinity water use [19]. Post-season leaching further reduces the soil salt content [50]. Under consecutive dry-year conditions, the seasonal irrigation volume is controlled within 216–240 mm. We set 3 g·L^{-1} as the baseline salinity, and a small number of irrigation applications can be adjusted to 2 g·L^{-1}; for normal water years, the seasonal irrigation quota is 168–192 mm, and the irrigation salinity remains steady at 3 g·L^{-1} for the entire growing period; when consecutive wet years occur, the total seasonal irrigation quota reduces to 72–96 mm, while the baseline salinity is maintained at 3 g·L^{-1}, with individual irrigation events permitted to reach 4 g·L^{-1} (Table 9). In addition, freshwater leaching every 10 years during the dormancy period [51] is recommended to maintain long-term salt equilibrium.

Table 9. Optimal irrigation scheme for long-term saline water drip irrigation based on the model.

Irrigation Event Growth Stage		Leaf Expansion Stage	Flowering and Fruiting Stage	Fruit Swelling Stage	Maturity Stage	Irrigation Quota/mm
Date		4/15–5/24	5/25–6/19	6/20–8/31	9/01–10/01	
Irrigation water quality	Wet year (Consecutive)	3(4)	3(4)	3(4)	3(4)	
	Normal water year	3	3	3	3	
	Dry year (Consecutive)	3(2)	3(2)	3(2)	3(2)	
Irrigation frequency	Wet year (Consecutive)	2–3			0–1	72–96
	Normal water year	3–4		1–2	1–2	168–192
	Dry year (Consecutive)	2	5–6		1–2	216–240
Single irrigation quota/mm				24		

4.4. Limitations and Future Research

Although the coupled MODFLOW and HYDRUS-2D framework effectively simulated long-term soil water–salt dynamics, several assumptions may introduce uncertainties into the predictions. The one-way coupling approach did not consider the feedback from soil water–salt transport to groundwater flow, while predefined soil hydraulic and root water uptake parameters may not fully capture their spatial and temporal variations under different salinity conditions. In addition, uncertainties in solute transport parameters and groundwater boundary conditions may affect long-term soil salinity predictions. Therefore, the sensitivity analysis of key model parameters is necessary to evaluate their influence on simulated soil salinity and the robustness of the proposed irrigation strategies. Although the 3 g·L^{-1} baseline irrigation salinity provided a relatively balanced option under the modeled conditions, its applicability may vary with soil properties, groundwater fluctuations, and rainfall distribution. Further sensitivity analysis and long-term field validation are needed to assess the reliability of the proposed irrigation strategies under different hydrological conditions.

5. Conclusions

The goal of this study was to utilize numerical models to assist farmers and managers in selecting the optimal saline irrigation management for jujube. A three-year field experiment was conducted to investigate the acceptable salinity level for the saline water irrigation of Ziziphus jujuba 'Dongzao'in the saline–alkali area of Yellow River Delta in China. The combined MODFLOW and HYDRUS numerical model method, which depicts the participation and influence of groundwater on the transport of water and salt in soil, was used for the long-term irrigation of jujube with saline water to evaluate the effect of irrigation water salinity on soil water and salt concentration in shallow buried areas. The conclusions are as follows:

(1) The results of the field experiment showed that the yield of Ziziphus jujuba 'Dongzao' decreased with increasing irrigation mineralization. The EC_e of the root zone was 12.64 dS·m^{-1} (0.27%) and 8.85 dS·m^{-1} (0.19%) when the relative yield decreased to 50% and 85%, respectively. In addition, the content of several quality indicators (i.e., soluble solids, reducing sugar, organic acid, and vitamin C) in the treatment with mineralization ≥ 4 g·L^{-1} was significantly higher than that in the control treatment.

(2) The MODFLOW and HYDRUS were used to simulate the soil water and salinity under groundwater table fluctuations. In the case of accurate calibration and high accuracy

field experiment data entry, the results of the physical model showed that, in the presence of shallow and saline groundwater, both the MODFLOW and HYDRUS model simulation results meet the basic accuracy requirements for simulation. Nevertheless, the predictive performance for soil salinity varies substantially across soil depths and irrigation treatments. These discrepancies reflect the inherent uncertainties in soil salinity simulation, which should be fully considered when extending the model outputs to long-term irrigation management.

(3) A decade-long simulation was conducted to evaluate the impacts of continuous irrigation using slightly saline water with varying mineralization levels on soil water and salt dynamics under real hydrological year conditions, based on the aforementioned model. Considering both the soil salinity dynamics and jujube production benefits, the recommended seasonal irrigation quota reaches 216–240 mm for consecutive dry years, where 3 $g \cdot L^{-1}$ is the baseline and 2 $g \cdot L^{-1}$ is acceptable for some irrigation events; the quota is 168–192 mm for normal water years with a consistent salinity of 3 $g \cdot L^{-1}$ for all irrigation events; for consecutive wet years, the seasonal irrigation quota is 72–96 mm, and we keep 3 $g \cdot L^{-1}$ as the baseline, with an upward adjustment to 4 $g \cdot L^{-1}$ available for selected irrigation events. Furthermore, it is recommended that, after approximately ten years of saline water irrigation, freshwater should be applied during the dormancy period of *Ziziphus jujuba* 'Dongzao' to leach excess salts from the soil profile.

Author Contributions: Conceptualization, X.C., Z.X. and G.P.; methodology, Z.X. and G.P.; software, X.C. and Y.X.; validation, R.W., Z.X. and G.P.; formal analysis, X.C.; investigation, X.C.; Y.X. and R.W.; writing—original draft, X.C., Y.X. and R.W.; writing—review and editing, Z.X. and G.P.; supervision, Z.X. and G.P.; funding acquisition, X.C. and Z.X. All authors have read and agreed to the published version of the manuscript.

Funding: This research was funded by the Key Research and Development Program of Shandong Province, China, grant number 2024CXGC010912; the Natural Science Foundation of Shandong Province, China, grant number ZR2025QC533; and the Doctoral Program of University of Jinan, grant number XBS2461.

Data Availability Statement: The data presented in this study are available in the article.

Conflicts of Interest: The authors declare no conflicts of interest.

References

1. Lei, S.; Jia, X.; Zhao, C.; Shao, M. A review of saline-alkali soil improvements in China: Efforts and their impacts on soil properties. *Agric. Water Manag.* **2025**, *317*, 109617. [CrossRef]
2. Gao, H.; Fu, T.; Tang, S.; Liu, J. Effects of saline water irrigation on winter wheat and its safe utilization under a subsurface drainage system in coastal saline-alkali land of Hebei Province, China. *Irrig. Sci.* **2023**, *41*, 251–260. [CrossRef]
3. Hou, G.; Gao, M.; Ye, S.; Zhao, G. Source of salt and the salinization process of shallow groundwater in the Yellow River Delta. *Earth Sci. Front.* **2022**, *29*, 145–154. [CrossRef]
4. Liu, Z.; Gao, C.; Yan, Z.; Shao, L.; Chen, S.; Niu, J.; Zhang, X. Effects of long-term saline water irrigation on soil salinity and crop production of winter wheat-maize cropping system in the North China Plain: A case study. *Agric. Water Manag.* **2024**, *303*, 109060. [CrossRef]
5. Gao, C.; Gao, Y.; Liu, X. The complete genome of Ziziphus jujuba cv. dongzao, an economic crop in Yellow River Delta of China. *Mitochondrial DNA B Resour.* **2017**, *2*, 692–693. [CrossRef]
6. Kanzari, S.; Šimůnek, J.; Daghari, I.; Younes, A.; Ali, K.B.; Mariem, S.B.; Ghannem, S. Modeling irrigation of tomatoes with saline water in semi-arid conditions using HYDRUS-1D. *Land* **2024**, *13*, 739. [CrossRef]
7. Guo, L.; Wang, Z.; Simunek, J.; He, Y.; Muhammad, R. Optimizing the strategies of mulched brackish drip irrigation under a shallow water table in Xinjiang, China, using HYDRUS-3D. *Agric. Water Manag.* **2023**, *283*, 108303. [CrossRef]
8. Lu, D.; Liu, L.; Bai, Y.; An, Q.; Cheng, Y.; Huang, G. Deficit irrigation alleviates the increase in soil salinity content in saline-alkali regions of China and improves irrigation water productivity: A meta-analysis. *Agric. Water Manag.* **2025**, *320*, 109872. [CrossRef]

9. Zhao, Q.; Xin, M.; Ai, P.; Ma, Y. Effects of continuous saline water irrigation on soil salinization characteristics and dryland jujube tree. *Agronomy* **2025**, *15*, 1898. [CrossRef]
10. Li, M.; Guo, Y.; Liu, S.; Zhao, Y.; Pang, X.; Li, Y. Autotetraploidization in Ziziphus jujuba Mill. var. spinosa enhances salt tolerance conferred by active, diverse stress responses. *Environ. Exp. Bot.* **2019**, *165*, 92–107. [CrossRef]
11. Wang, Y.; Shi, W.; Jing, B. Optimizing brackish water and nitrogen application regimes for soil salinity, yield, fertilizer and water productivity of a mulched drip irrigated cotton cropping system. *Field Crops Res.* **2023**, *302*, 109097. [CrossRef]
12. Wang, R.; Cao, H.; Kang, S.; Du, T.; Tong, L.; Kang, J.; Gao, J.; Ding, R. Agronomic measures improve crop yield and water and nitrogen use efficiency under brackish water irrigation: A global meta-analysis. *Agric. Syst.* **2025**, *226*, 104304. [CrossRef]
13. Guo, L.; Yu, H.; Zhang, C.; Kharbach, M. The role of phytohormones in alleviating salt stress in rice. *Phyton-Int. J. Exp. Bot.* **2024**, *93*, 3131–3149. [CrossRef]
14. Li, W.; Kang, S.; Du, T.; Ding, R.; Zou, M. Optimal groundwater depth and irrigation amount can mitigate secondary salinization in water-saving irrigated areas in arid regions. *Agric. Water Manag.* **2024**, *302*, 109007. [CrossRef]
15. Liu, B.; Wang, S.; Liu, X.; Sun, H. Evaluating soil water and salt transport in response to varied rainfall events and hydrological years under brackish water irrigation in the North China Plain. *Geoderma* **2022**, *422*, 115954. [CrossRef]
16. Xu, Y.; Liu, Z.; Cheng, H.; Zhu, X.; Huang, S.; Li, Z. Simulation of water and salt transportation under border irrigation in field scale based on HYDRUS-3D. *Water Resour. Hydropower Eng.* **2021**, *52*, 14–22. [CrossRef]
17. Šimůnek, J.; van Genuchten, M.T.; Šejna, M. Recent developments and applications of the HYDRUS computer software packages. *Vadose Zone J.* **2016**, *15*, 1–25. [CrossRef]
18. Simunek, J.; Sejna, M.; van Genuchten, M.T. New features of version 3 of the HYDRUS (2D/3D) computer software package. *J. Hydrol. Hydromech.* **2018**, *66*, 133–142. [CrossRef]
19. Zhang, Y.; Li, X.; Simunek, J.; Shi, H.; Chen, N.; Hu, Q. Optimizing drip irrigation with alternate use of fresh and brackish waters by analyzing salt stress: The experimental and simulation approaches. *Soil Tillage Res.* **2022**, *219*, 105355. [CrossRef]
20. Li, X.; Li, Z.; Fu, W.; Li, F. The influence of shallow groundwater on the physicochemical properties of field soil, crop yield, and groundwater. *Agriculture* **2024**, *14*, 341. [CrossRef]
21. Varouchakis, E.A.; Karatzas, G.P.; Giannopoulos, G.P. Impact of irrigation scenarios and precipitation projections on the groundwater resources of Viannos Basin at the island of Crete, Greece. *Environ. Earth Sci.* **2015**, *73*, 7359–7374. [CrossRef]
22. Liu, Q.; Mou, X.; Cui, B.; Ping, F. Regulation of drainage canals on the groundwater level in a typical coastal wetlands. *J. Hydrol.* **2017**, *555*, 463–478. [CrossRef]
23. Luo, F.; Wang, D.; Tian, X.; Bi, X.; Zheng, Q.; Zhou, Z.; Tang, Z. Estuarine groundwater level response to and recovery from extreme precipitation events: Typhoon Lekima in the Yellow River Delta. *J. Hydrol.* **2024**, *632*, 130918. [CrossRef]
24. Yu, J.; Li, Y.; Han, G.; Zhou, D.; Fu, Y.; Guan, B.; Wang, G.; Ning, K.; Wu, H.; Wang, J. The spatial distribution characteristics of soil salinity in coastal zone of the Yellow River Delta. *Environ. Earth Sci.* **2014**, *72*, 589–599. [CrossRef]
25. Wang, T.; Wang, J.; Xu, Z.; Pang, G.; Liu, J. Effects of saline water irrigation on water-salt dynamic in root district and winter jujube yield. *Water Sav. Irrig.* **2017**, *6*, 46–49+54.
26. Bao, S. *Soil and Agricultural Chemistry Analysis*; China Agriculture Press China Agriculture Press: Beijing, China, 2000; pp. 178–200.
27. Rhoades, J. Soluble salts. In *Methods of Soil Analysis, Part 2. Chemical and Microbiological Properties*, 2nd ed.; Page, A.L., Ed.; Agronomy Monograph No. 9; ASA; SSSA: Madison, WI, USA, 1982; pp. 167–179.
28. Allen, R.G.; Pereira, L.S.; Raes, D.; Smith, M. *Crop Evapotranspiration-Guidelines for Computing Crop Water Requirement*; Irrigation and Drainage Paper No. 56; Food and Agriculture Organization of the United Nations: Rome, Italy, 1998; p. 24.
29. Wei, Q.; Fei, L. Study on the water consumption rules and crop coefficient of drip-irrigation jujube trees in the mountain areas of North Shanxi Province. *Subtrop. Soil Water Conserv.* **2012**, *24*, 12–16.
30. Maas, E.V.; Hoffman, G.J. Crop salt tolerance-Current assessment. *J. Irrig. Drain. Div.* **1977**, *103*, 115–134. [CrossRef]
31. Van Genuchten, M.T. A closed-form equation for predicting the hydraulic conductivity of unsaturated soils. *Soil Sci. Soc. Am. J.* **1980**, *44*, 892–898. [CrossRef]
32. Jiang, X.; Lin, H.; Shi, J.; Neethirajan, S.; Lin, Y.; Chen, Y.; Wang, H.; Lin, Y. Effects of a novel chitosan formulation treatment on quality attributes and storage behavior of harvested litchi fruit. *Food Chem.* **2018**, *252*, 134–141. [CrossRef]
33. Šimůnek, J.; van Genuchten, M.T.; Šejna, M. *The HYDRUS Software Package for Simulating Two- and Three-Dimensional Movement of Water, Heat, and Multiple Solutes in Variably-Saturated Media, Technical Manual, Version 1.0*; PC Progress: Prague, Czech Republic, 2006; p. 241.
34. Feddes, R.A.; Kowalik, P.J.; Zaradny, H. *Simulation of Field Water Use and Crop Yield*; Centre for Agricultural Publishing and Documentation: Wageningen, The Netherlands, 1978; pp. 197–198.
35. Ma, Z.; Liu, J.; Wen, Y.; Zhang, J.; Yin, F.; Guo, L.; Li, W.; He, J.; Ma, J.; Liang, Y.; et al. Optimizing cotton yield through appropriate irrigation water salinity: Coordinating above- and below-ground growth and enhancing photosynthetic capacity. *Eur. J. Agron.* **2024**, *154*, 127095. [CrossRef]

36. Liu, G.; Wilson, B.; Bohling, G.; Whittemore, D.; Butler, J., Jr. Estimation of specific yield for regional groundwater models: Pitfalls, ramifications, and a promising path forward. *Water Resour. Res.* **2022**, *58*, 245379283. [CrossRef]
37. Sun, D.; Luo, N.; Vandenhoff, A.; McCall, W.; Zhao, Z.; Wang, C.; Rudolph, D.; Illman, W. Evaluation of Hydraulic Conductivity Estimates from Various Approaches with Groundwater Flow Models. *Groundwater* **2023**, *62*, 384–404. [CrossRef]
38. Awais, M.; Arshad, M.; Ahmad, S.; Nazeer, A.; Waqas, M.; Aziz, R.; Shakoor, A.; Rizwan, M.; Chauhdary, J.; Mehmood, Q.; et al. Simulation of groundwater flow dynamics under different stresses using MODFLOW in Rechna Doab, Pakistan. *Sustainability* **2023**, *15*, 661. [CrossRef]
39. Phogat, V.; Mahadevan, M.; Skewes, M.; Cox, J.W. Modelling soil water and salt dynamics under pulsed and continuous surface drip irrigation of almond and implications of system design. *Irrig. Sci.* **2012**, *30*, 315–333. [CrossRef]
40. Ma, L.; Wei, G.; Wang, T.; Ma, Y. Numerical simulation of young jujube root characteristics under drip irrigation in arid area based on Feddes model. *Water Sav. Irrig.* **2016**, *247*, 11–14.
41. Karandish, F.; Simůnek, J. An application of the water footprint assessment to optimize production of crops irrigated with saline water: A scenario assessment with HYDRUS. *Agric. Water Manag.* **2018**, *208*, 67–82. [CrossRef]
42. Zhang, H.; Ding, J.; Wang, Y.; Zhou, D.; Zhu, Q. Investigation about the correlation and propagation among meteorological, agricultural and groundwater droughts over humid and arid/semi-arid basins in China. *J. Hydrol.* **2021**, *603*, 127007. [CrossRef]
43. *T/BZFS 001-2021*; Technical Regulations for Irrigation, Drainage and Waterproofing in Winter Jujube Orchards. Binzhou Forestry Society: Binzhou, China, 2021.
44. Feng, G.; Zhu, C.; Wu, Q.; Wang, C.; Zhang, Z.; Mwiya, R.; Zhang, L. Evaluating the impacts of saline water irrigation on soil water-salt and summer maize yield in subsurface drainage condition using coupled HYDRUS and EPIC model. *Agric. Water Manag.* **2021**, *258*, 107175. [CrossRef]
45. Asadbegi, M.; Bahmani, O.; AtlassiPak, V. Impact of saline water on some ions uptake and yield of wheat genotypes and soil salt accumulation. *Commun. Soil Sci. Plant Anal.* **2019**, *50*, 2787–2796. [CrossRef]
46. Wang, Q.; Xu, J.; Li, D.; Zhou, Y.; Chen, M.; Zhang, X.; Zhang, J.; Zhao, B. Brackish water irrigation-induced recruitment of specific consortium determines microbial resistance that facilitates crop yield in a field experiment. *Pedosphere* **2024**, *35*, 820–833. [CrossRef]
47. Martínez-Moreno, A.; Pérez-Alvarez, E.P.; Intrigliolo, D.S.; Mirás-Avalos, J.M.; López-Urrea, R.; Gil-Muñoz, R.; Lizama, V.; García-Esparza, M.J.; Alvarez, M.; Buesa, I. Effects of deficit irrigation with saline water on yield and grape composition of *Vitis vinifera* L. cv. Monastrell. *Irrig. Sci.* **2022**, *41*, 469–485. [CrossRef]
48. Li, S.; Luo, Z.; Jia, Z.; Tang, S.; Wu, D. An analytical model for studying the effect of rainfall on salt leaching under controlled drainage in subhumid irrigation areas. *J. Hydraul. Eng.* **2015**, *46*, 127–137. [CrossRef]
49. Ma, J.; Liu, J.; Wen, Y.; Ma, Z.; Zhang, J.; Yin, F.; Javed, T.; Zhang, J.; Wang, Z. Enhancing the yield and water use efficiency of processing tomatoes (Lycopersicon esculentum Miller) through optimal irrigation and salinity management under mulched drip irrigation. *J. Integr. Agric.* **2025**, *24*, 2410–2424. [CrossRef]
50. Wang, Z.; Jin, M.; Šimůnek, J.; van Genuchten, M.T. Evaluation of mulched drip irrigation for cotton in arid Northwest China. *Irrig. Sci.* **2014**, *32*, 15–27. [CrossRef]
51. *DB37/T 1640.2-2018*; Shandong Province Main Crop Irrigation Quota—Part 2: Main Vegetables and Fruit Trees. Shandong Provincial Market Supervision Administration: Jinan, China, 2018.

Disclaimer/Publisher's Note: The statements, opinions and data contained in all publications are solely those of the individual author(s) and contributor(s) and not of MDPI and/or the editor(s). MDPI and/or the editor(s) disclaim responsibility for any injury to people or property resulting from any ideas, methods, instructions or products referred to in the content.